Journal of Computational Electronics (2021) 20:1043–1049
https://doi.org/10.1007/s10825-020-01641-z

Compact modeling of metal-oxide TFTs based on artificial neural network and improved particle swarm optimization

Wanling Deng[1] · Wanqin Zhang[1] · You Peng[1] · Weijing Wu[2] · Junkai Huang[1] · Zhi Luo[1]

Received: 3 November 2020 / Accepted: 19 December 2020 / Published online: 20 January 2021

Abstract
The application of artificial neural network (ANN) can give a very accurate and fast model for semiconductor devices used in circuit simulations. In this paper, we have applied multi-layer perceptron (MLP) neural network based on limited memory Broyden–Fletcher–Goldfarb–Shanno (L-BFGS) method to model the flexible metal-oxide thin-film transistors (TFTs). An improved particle swarm optimization (PSO) is employed to find suitable initial parameters for the ANN model, which consists of a centroid opposition-based learning algorithm and a mutation strategy based on Euclidean distance to enhance the searching ability further. This hybrid modeling routine can improve the accuracy of predictions of both the *I*–*V* and small signal parameters (g_d, g_m, etc.) characteristics, which are in good agreement with experimental data and fully demonstrate the validity of the proposed model. Furthermore, the model is implemented into a simulator with Verilog-A. The circuit-level tests of TFT show that the ANN compact model with PSO enables accurate performance estimation of metal-oxide TFT circuits.

Keywords Particle swarm optimization (PSO) · Limited memory Broyden–Fletcher–Goldfarb–Shanno (L-BFGS) · Metal-oxide thin-film transistors

1 Introduction

Recently, flexible metal-oxide thin-film transistors (TFTs) have attracted much attention due to their excellent characteristics such as high mobility, controllable conductivity, good uniformity, and lower process temperature [1, 2]. Therefore, they are considered as the most promising technology for flexible electronics [3, 4]. The design of TFT-based circuits places great demand for computer-aided design (CAD) tools. And CAD requires fast, accurate, and robust device compact models. In the past few years, many models [5, 6] based on the physical properties of metal-oxide TFTs have been reported. Though traditional physical models are considered to be accurate and describe the underlying device physics, it cannot be denied that they are usually complex and take significant time to develop [7]. To catch up with the rapid technology development and evaluate the advantages of many emerging devices, a good alternative might be the use of the models generated by the artificial neural networks (ANN) [8]. Therefore, an improved ANN model is proposed in this paper for metal-oxide TFTs, which is solely based on data measurements and can be obtained in a short time without going into the detailed device physics.

The multi-layer perceptron (MLP) is one of multi-layer feedforward neural networks [9]. In comparison with other different ANNs, like radial basis functions (RBF) and least squares-support vector machine (LS-SVM), the MLP achieves a good degree of accuracy with less complexity [10]. As a universal approximator [9], MLP models provide continuous and smooth approximations over the entire operation regions of a transistor from subthreshold to strong inversion. Because of its simplicity and high efficiency, MLP can be regarded as a potential method to build compact models for semiconductor devices. In this work, MLP is adopted for modeling metal-oxide TFTs, and the limited memory Broyden–Fletcher–Goldfarb–Shanno (L-BFGS) method [11] is applied for MLP to update the weights and biases. L-BFGS is efficient but very sensitive to the initial values. The initial weights and biases of MLP are randomized, which may converge to a local best

✉ Zhi Luo
zhluocn@gmail.com

[1] Department of Electronic Engineering, Jinan University, Guangzhou 510630, People's Republic of China

[2] State Key Laboratory of Luminescent Materials and Devices, South China University of Technology, Guangzhou 510640, People's Republic of China

solution due to the sensitivity of L-BFGS to initial values. Hence, it will result in inaccurate modeling results.

To address this problem, a particle swarm optimization (PSO) [12] is employed to initialize the weights and biases of MLP [13, 14]. The PSO has an excellent global searching ability so that it is suitable to search a hopeful initial position for L-BFGS method. However, one problem found in the standard PSO is that it could easily fall into local optima in many optimization problems [14]. In this paper, an improved centroid opposition-based learning PSO (COBPSO) algorithm with a mutation strategy based on Euclidean distance is proposed. It avoids premature convergences and allows particle swarm to continuously search for global optima by applying opposition-based learning [14, 15]. Besides it, the particle can be replaced by a new one to search the other area in solution space to enhance the searching ability further. Finally, for IZO TFTs, both the device and circuit-level tests show that the proposed scheme using hybrid modeling routine can reproduce and predict various devices and circuits with high accuracy.

2 Prediction technique

2.1 MLP model

In our previous work [16], we used the MLP neural network based on the L-BFGS algorithm for modeling, which is also adopted here as the basis of this paper. In [16], we define the neural-network training error (*loss*1) as

$$\text{loss1} = \frac{1}{n}\sum_{i=1}^{n}(\log(I_{\text{ds}}) - \log(I_{\widetilde{\text{ds}}}))^2 \tag{1}$$

where I_{ds} is the drain current training data, $I_{\widetilde{ds}}$ is the prediction value and n is the total amount of training dataset. Equation (1) is also the objective function of the MLP in [16].

However, this objective function lacks consideration of small signal parameters (i.e., g_m and g_d), which have a great influence on small-signal behaviors. The negative transconductances and output conductances may lead to non-convergence issues in circuit simulators [17]. Therefore, we have added the error of the small signal parameters into objective function in this paper to improve the accuracy of the complete model. With f as the output and Inj as the jth input of the jth neuron, the g_m and g_d can be obtained by the chain rule [17]:

$$\frac{\partial f}{\partial \text{In}j} = w_{kp}^3 \cdot [g_2' \cdot (w_{jk}^2 \cdot g_1' \cdot w_{ij}^1)] \tag{2}$$

where g_1 and g_2 are the first and second hidden layer activation functions, respectively; w_{ij}^1, w_{jk}^2 and w_{kp}^3 are the node weights of the first hidden, second hidden and output layers, respectively; and the node's index is shown by the subscripts. The improved objective function (loss) can be rewritten as:

$$\text{loss2} = \frac{1}{n}\sum_{i=1}^{n}\{w_{kp}^3 \cdot [g_2' \cdot (w_{jk}^2 \cdot g_1' \cdot w_{ij}^1)]\text{flag}_1 - g_d\}^2 \tag{3}$$

$$\text{loss3} = \frac{1}{n}\sum_{i=1}^{n}\{w_{kp}^3 \cdot [g_2' \cdot (w_{jk}^2 \cdot g_1' \cdot w_{ij}^1)]\text{flag}_2 - g_m\}^2 \tag{4}$$

$$\text{loss} = \text{loss1} + \text{loss2} + \text{loss3} \tag{5}$$

where flag_1 and flag_2 are two flag bits that are used to judge whether the data belongs to output or transfer characteristics. Then, the L-BFGS algorithm will update the weights and biases of each layer iteratively according to the new loss.

2.2 PSO based on centroid opposition-based learning

Opposition-based learning (OBL) [18] is introduced by Tizhoosh which has been proven to be an efficient method in many optimization problems [19]. To achieve a more accurate approximation for the optimization problem, the main idea of OBL is the simultaneous consideration of a solution and its corresponding opposite solution. In centroid opposition-based learning (COBL) [20], the opposite point is calculated by the centroid of the swarm to make full use of the group experience. Assuming (X_1, X_2,..., X_m) as m particles in a search space, the centroid of the swarm can be defined as follows:

$$M = \frac{1}{m}\sum_{i=1}^{m} X_i. \tag{6}$$

The opposite point of X_i is calculated as

$$OX_i = kM - X_i \tag{7}$$

$$k = 1 + \text{rand} \tag{8}$$

where rand is a random number uniformly distributed in [0, 1] as constriction factors to improve the diversity of particles. For the sake of accelerating convergence, the dynamic boundary is exploited to keep reducing the searching space of each particle. For $X_i = (x_{i1}, x_{i2},..., x_{iD})$, the dynamic boundary $[a, b]$ can be expressed as

$$a_j = \min(x_{ij}), b_j = \max(x_{ij}) \tag{9}$$

where j is a randomly chosen parameter index and x_{ij} is the j dimension of X_i. The particle's position will be reset when the particle meets the boundary. The update of particles crossed the dynamic boundary is given by

$$ox_{ij} = \begin{cases} a_j + \text{rand} \cdot (M_j - a_j) & ox_{ij} < a_j \\ M_j + \text{rand} \cdot (b_j - M_j) & ox_{ij} > b_j. \end{cases} \quad (10)$$

The same as MLP, the mean square error between model predictive value and experimental data is defined as the fitness function of PSO. The fitness function makes the movement of each particle more directional to reach the minimum. The positions of particles are updated by tracking their own optimum p_{best} and swarm's optimum g_{best}. For updating velocities and positions, we obtain [12]

$$V_{ij} = wV_{ij} + r_{i1} \cdot c_1(p_{\text{best}} - x_{ij}) + r_{i2} \cdot c_2(g_{\text{best}} - x_{ij}) \quad (11)$$

$$x_{ij} = x_{ij} + V_{ij} \quad (12)$$

where V_{ij} and x_{ij} are the velocity and position of the ith particle, respectively; w is an inertia factor describing the contribution rate of the particle's previous speed to its current speed, which helps particles to search a wider area in the previous direction. In addition, r_{i1} and r_{i2} are two random numbers in the range of [0,1]; c_1 and c_2 are the acceleration factors. The PSO has the advantage of rapid convergence and the ability to search optimal solutions within global space. The parameter extraction routines based on PSO are convenient and efficient [21]. After introducing COBL into PSO, the fitness value of the current particle and the opposite point of this particle will be compared, and then a better point can be selected. However, in the later stage of this algorithm, all particles will gather more and more, which may lead to a local optimum. Hence, to enhance the global search ability of algorithm, a strategy of mutation based on Euclidean distance is adopted to particle swarm, which is shown in Fig. 1.

After 100 iterations, the Euclidean distance (Edis_i) from each particle to g_{best} can be calculated as

$$\text{Edis}_i = \sqrt{\sum_{j=1}^{D} (x_{ij} - g_{\text{best}j})^2}. \quad (13)$$

And the average Euclidean distance (Edis_a) from the entire population to g_{best} is obtained as

$$\text{Edis\_}a = \frac{1}{m} \sum_{i=1}^{m} \text{Edis}_i. \quad (14)$$

When the distance between particle X_i and g_{best} is less than Edis_a, X_i has a certain chance to mutate into random search particles. Particles with a distance from g_{best} less than Edis_a will be assigned a random number c which is between [0,1]. As shown in Fig. 1, when c is larger than 0.5, the particle will mutate into a random particle. The mutation process is completely random, so the particles may still fall in the area close to g_{best}. From the perspective of searching, the strategy

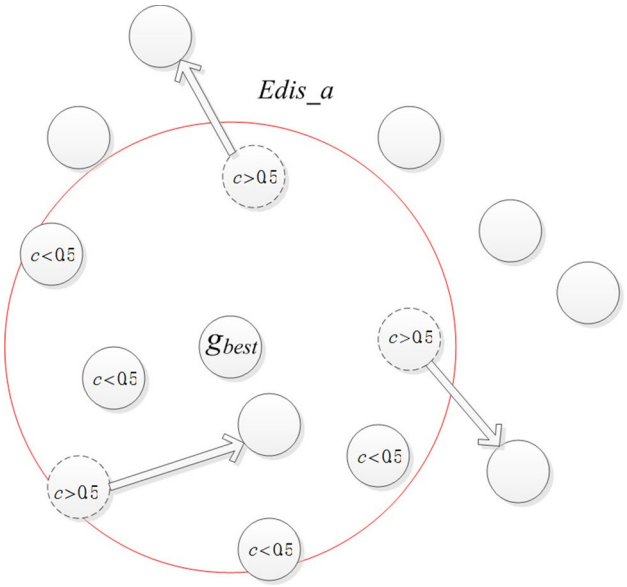

Fig. 1 Schematic diagram of mutation strategy. The white circles depict particles, and Edis_a represents the distance from the red line to g_{best} (Color figure online)

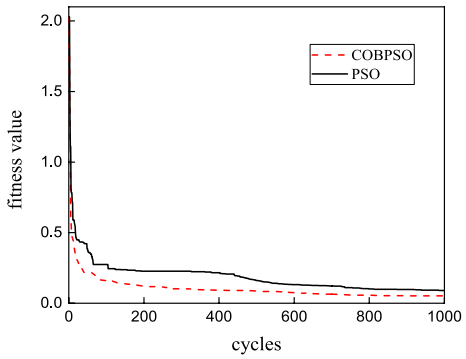

Fig. 2 Comparison results of COBPSO and standard PSO

replaces half of the particles closer to g_{best} by new particles to search for other solutions. From the perspective of convergence, this method makes the rest particles continue to move towards g_{best}, so that they can converge to local minimum. The proposed algorithm has been tested on IEEE Congress on Evolutionary Computation (CEC) 2013 test functions. Comparisons have been conducted between our proposed algorithm (COBPSO) and standard PSO, which is demonstrated in Fig. 2. It shows that our algorithm has a more powerful global searching ability.

2.3 The hybrid algorithm

An MLP optimized by COBPSO is adopted in the metal-oxide TFTs' modeling. The mean square error of predict value and experimental data is set as the objective function

of both L-BFGS and COBPSO. Suitable initial parameters of MLP can be found by COBPSO to overcome the main drawback of L-BFGS. Then, the parameters of MLP are updated by L-BFGS, thereby improving the model's accuracy and generalization ability. Figure 3 plots the flowchart of this hybrid algorithm. In [16], if the accuracy of the modeling result is not up to standard, the neural network will restart training. Different from that, in this paper, if the accuracy is not enough after the training, the obtained parameter value will be returned to the PSO as the initial one, and thus, it improves the efficiency of the entire modeling.

3 Verification and discussions

3.1 Accuracy verification

As a kind of metal-oxide TFTs, IZO TFTs were fabricated to obtain experimental data, which is shown in Fig. 4. With the channel length is fixed to 5 µm, multiple TFTs with widths of 5, 10, 15, 20, 30, 40, 50, 75, and 100 µm are sampled to build MLP model. The fabrication of the devices can be found in [22]. In addition, the data of output characteristics are sampled at unequal intervals. Smaller steps in the subthreshold regime are usually helpful for improving model's accuracy. In this work, the interval of the region of $V_{DS} < 3$ V is 0.05 V, and the other is 0.1 V.

The MLP with two hidden layers can realize the compact modeling of transistors [2, 8]. The most suitable structure of MLP (3-15-20-1) (represents 3 inputs, 15 neurons in the first hidden layer, 20 neurons in the second hidden layer, and 1 output) is judged by a trial-and-error process, the accuracy of which can be over 97.5%. As shown in Fig. 5, we put the same data set into MLP and COBPSO-MLP to train separately and compare the modeling results of these two models to verify the effectiveness of our proposed modeling method. Generally, MLP method can work for modeling the *I-V* characteristics, but g_d and g_m obtained by MLP (solid lines in Fig. 5) cannot match well with experimental data. This problem is caused by MLP falling into local optimum. The modeling results will not be ideal if L-BFGS is not given appropriate initial values. However, by introducing COBPSO to MLP, the results of g_d and g_m become much better, which fully proves the validity of our proposed modeling method. Our proposed hybrid algorithm combines the advantages of both global searching ability from COBPSO and local convergence ability from L-BFGS algorithm.

3.2 Implementation and circuit applications

To confirm the applicability of the COBPSO-MLP model, it was implemented in the form of Verilog-A and then embedded in a SPICE simulator. First, this model was put into a double-stages inverter circuit [23] based on IZO TFTs for DC simulation, whose schematic is shown in Fig. 6a. The related parameters of the devices used in the inverter are shown in Table 1. This inverter was fabricated, and we measured the voltage-transfer characteristics, which are demonstrated in Fig. 6b. The DC simulation results of the inverter are also shown and compared with experimental data. From Fig. 6, one can see that the simulation results of double-stages inverter with COBPSO-MLP model are in good

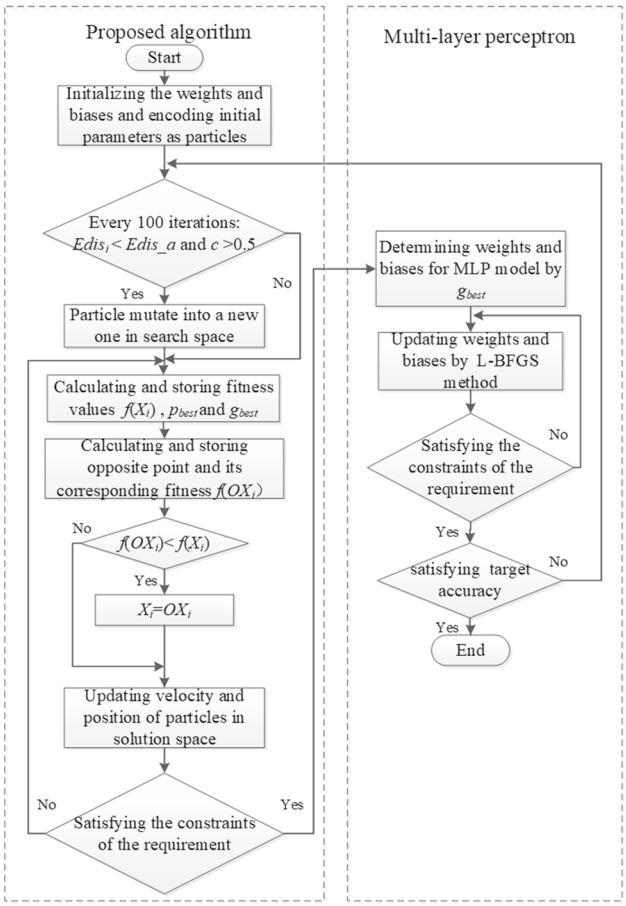

Fig. 3 The flowchart of the hybrid algorithm

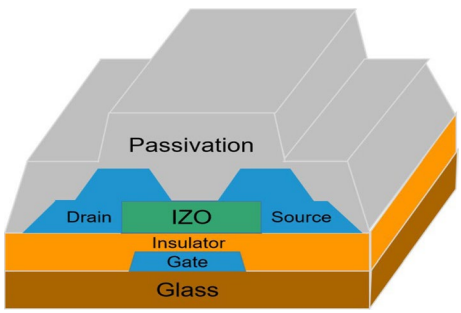

Fig. 4 Schematic diagram of an IZO-TFT

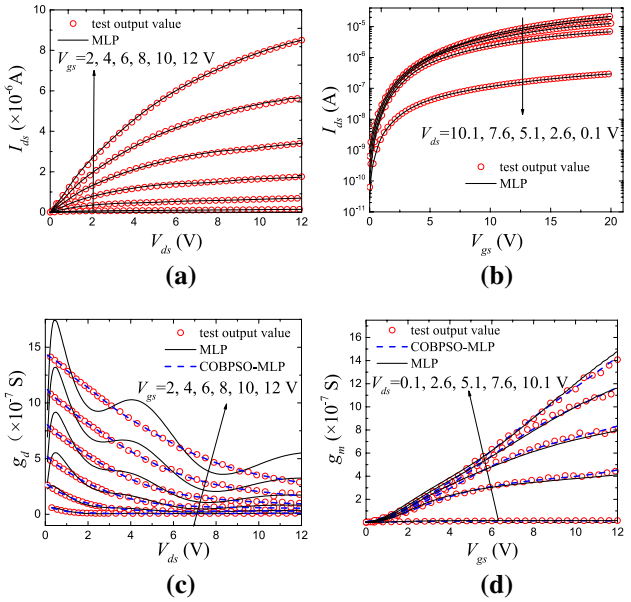

Fig. 5 Simulation results of the MLP and COBPSO-MLP models with channel width of 5 µm. **a** Output characteristics. **b** Transfer characteristics. **c** Output conductance (g_d). **d** Transconductance (g_m)

Table 1 Information about the devices used in Fig. 6

Devices used in inverter	Double-stages inverter
M1(W/L)	10 µm/5 µm
M2(W/L)	20 µm/5 µm
M3(W/L)	15 µm/5 µm
M4(W/L)	30 µm/5 µm
C1	0.5 pF

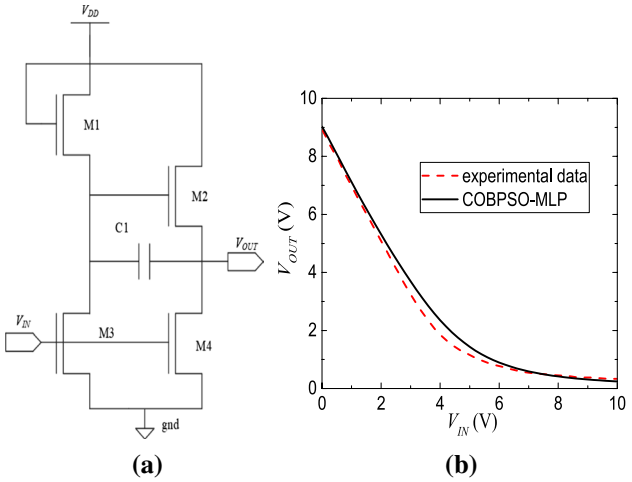

Fig. 6 Double-stages inverter. **a** Schematic diagram [23]. **b** Comparison results between experimental data and the COBPSO-MLP output value of the double-stages inverter

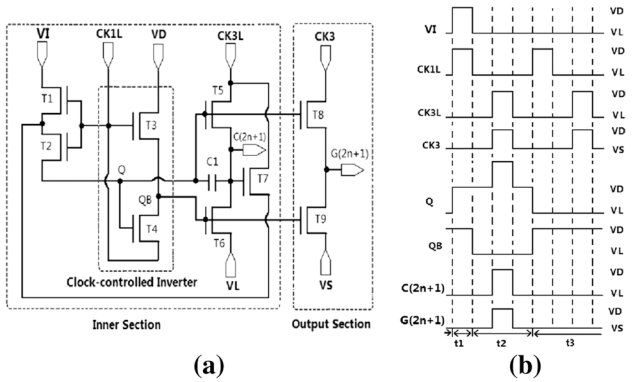

Fig. 7 The clock-controlled inverter type row drive circuit [24]. **a** Schematic diagram. **b** Voltage timing diagram

agreement with experimental data in a wide range of operation regions. It can be noticed that there are some errors in the transition region, but the maximum output voltage (V_{OH}) and the minimum output voltage (V_{OL}) are accurately estimated. As a result, we believe that the basic accuracy of the circuit simulation can be guaranteed by COBPSO-MLP model.

Moreover, we adopted a more complex scan driver with a clock-controlled inverter [24] to further verify our proposed model, which is shown in Fig. 7. The relevant parameters of the circuit are the same as those in [24]. In Fig. 8, the RPI [25] and COBPSO-MLP models were put into the circuit for transient simulation separately. In order to conduct transient simulation of the circuits, we also use the same hybrid modeling scheme to predict the *C–V* characteristics. The RPI model which is commonly used in the industrial design process is employed here for comparison with the ANN model. It can be seen that the prediction values of the COBPSO-MLP model at each node agree well with RPI model as a whole and the dynamic characteristics of the circuit can be captured, which further proves the effectiveness of our proposed modeling scheme. However, RPI model has some limitations. For example, formulation is based on regional approach and simulation convergence cannot be guaranteed. In addition, some specific features of TFT devices were not taken into account in RPI model. Therefore, the RPI model cannot fully predict the characteristics of MOTFTs. As a result, it can be concluded that the ANN modeling method is an effective tool for compact modeling and the COBPSO-MLP model proposed in this paper is suitable for being applied in circuit simulation and optimization process.

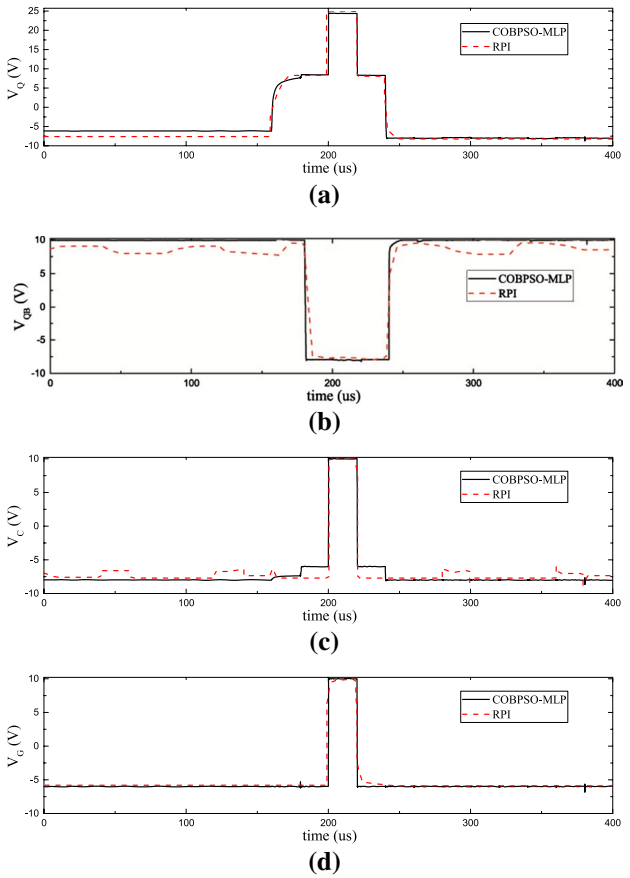

Fig. 8 Comparison results between simulation results with the COBPSO-MLP and RPI models. **a** V_Q. **b** V_{QB}. **c** V_C. **d** V_G

4 Conclusion

A COBPSO-MLP modeling method for metal-oxide TFTs is implemented in this paper. COBL and a mutation strategy are introduced to the standard PSO algorithm, which enhances the efficiency of standard PSO. This modeling scheme involving the COBPSO and L-BFGS methods has the advantages of both algorithms. The *I–V* characteristics and small signal parameters (g_d and g_m) match well with experimental data. Moreover, the model is implemented in Verilog-A and tested for various circuits. With its accuracy and efficiency, extensive device- and circuit-level simulations show that the proposed model is suitable for evaluation of metal-oxide TFT-based flexible circuits.

Acknowledgements The authors would like to thank New Vision Opto-Electronic Technology Co., Ltd., China, for data support of IZO-TFT devices and circuits. This work was supported by the Guangdong Natural Science Foundation under Grants 2018A030313018 and 2020A1515010567.

References

1. Zhang, L., Huang, C., Li, G., Zhou, L., Wu, W., Xu, M., Wang, L., Ning, H., Yao, R., Peng, J.: A low-power high-stability flexible scan driver integrated by IZO TFTs. IEEE Trans. Electron. Devices **63**(4), 1779–1782 (2016)
2. Jeong, J.K.: The status and perspectives of metal oxide thin-film transistors for active matrix flexible displays. Semicond. Sci. Technol. **26**(3), 034008 (2011)
3. Fang, J., Deng, W., Ma, X., Huang, J., Wu, W.: A surface-potential-based DC model of amorphous oxide semiconductor TFTs including degeneration. IEEE Electron Device Lett. **38**(2), 183–186 (2017)
4. He, H., He, J., Deng, W., Wang, H., Liu, Y., Zheng, X.: Trapped-charge-effect-based above-threshold current expressions for amorphous silicon TFTs consistent with Pao-Sah model. IEEE Trans. Electron Devices **61**(11), 3744–3750 (2014)
5. Tsormpatzoglou, A., Hastas, N.A., Choi, N., Mahmoudabadi, F., Hatalis, M.K., Dimitrialdis, C.A.: Analytical surface potential-based drain current model for amorphous InGaZno thin film transistors. J. Appl. Phys. **114**(18), 184502–1845026 (2013)
6. Garcia, R., Mejia, I., Tinoco, J., et al.: A compact drain current model for thin-film transistor under bias stress condition. IEEE Trans. Electron Devices **65**(5), 1803–1809 (2018)
7. Bahubalindrun, P., Tavares, V., Barquinha, P., Oliveira, P., Martins, R., Fortunato, E.: InGaZnO TFT behavioral model for IC design. Analog Integr. Circuits Signal Process. **87**(1), 73–80 (2016)
8. Hayati, M., Rezaei, A., Seifi, M.: CNT-MOSFET modeling based on artificial neural network: application to simulation of nanoscale circuits. Solid-State Electron. **54**(1), 52–57 (2010)
9. Hornik, K., Stinchcombe, M., White, H.: Multilayer feedforward networks are universal approximators. Neural Netw. **2**(5), 359–366 (1989)
10. Tavares, V., Candido, D., Barquinha, P.: a-GIZO TFT neural modeling, circuit simulation and validation. Solid State Electron. **105**, 30–36 (2015)
11. Liu, D., Nocedal, J.: On the limited memory BFGS method for large scale optimization. Math. Program. **45**(1), 503–528 (1989)
12. Eberhart, R., Kennedy, J.: A new optimizer using particle swarm theory. In: Proceedings of the Sixth International Symposium on Micro Machine and Human Science, pp. 39–43 (1995)
13. Ismail, A., Jeng, D.S., Zhang, L.: An optimised product-unit neural network with a novel PSO-BP hybrid training algorithm: applications to load-deformation analysis of axially loaded piles. Eng. Appl. Artif. Intell. **26**(10), 2305–2314 (2013)
14. Hou, C., Yu, X., Cao, Y., Lai, C., Cao, Y.: Prediction of synchronous closing time of permanent magnetic actuator for vacuum circuit breaker based on PSO-BP. IEEE Trans. Dielectr. Electr. Insul. **24**(6), 3321–3326 (2017)
15. Wang, H., Li, H., Liu, Y., Li, C., Zeng, S.: Opposition-based particle swarm algorithm with Cauchy mutation. In: IEEE Congress on Evolutionary Computation, pp. 25–28 (2007)
16. Peng, Y., Deng, W., Wu, W., Luo, Z., Huang, J.: Hybrid modeling routine for metal-oxide TFTs based on particle swarm optimization and artificial neural network. Electron. Lett. **56**(9), 453–456 (2020)
17. Zhang, L., Chan, M.: Artificial neural network design for compact modeling of generic transistors. J. Comput. Electron. **16**(3), 825–832 (2017)
18. Tizhoosh, H.: Opposition-based learning: a new scheme for machine intelligence. In: Conference on Intelligent Agents, Web Technologies and Internet Commerce. **1**, pp. 695–701 (2005)

19. Xu, Q., Wang, L., Hei, X., Zhao, L.: A review of opposition-based learning from 2005 to 2012. Eng. Appl. Artif. Intell. **29**(3), 1–12 (2014)
20. Rahnamayan, S., Jesuthasan, J., Bourennani, F., Salehinejad, H.: Computing opposition by involving entire population. In: IEEE Congress on Evolutionary Computation, pp. 6–11 (2014)
21. Wei, T., Yu, F., Huang, G., Xu, C.: A particle-swarm-optimization-based parameter extraction routine for three-diode lumped parameter model of organic solar cells. IEEE Electron Devices Lett. **40**(9), 1511–1514 (2019)
22. Chen, Z., Xu, W., Wu, J., Zhou, L., Wu, W., Zhao, J.: A new high gain operational amplifier using transconductance-enhancement topology integrated with metal oxide TFTs. IEEE J. Electron Devices Soc. **7**(1), 111–117 (2018)
23. Huang, T., Fukuda, K., Lo, C., Yeh, Y., Sekitani, T., Someya, T., Cheng, L.: Pseudo-CMOS: a design style for low-cost and robust flexible electronics. IEEE Trans. Electron. Devices **58**(1), 141–150 (2011)
24. Wu, W., Li, G., Xia, X., Zhang, L., Zhou, L., Xu, M., Wang, L.: Low-power bi-side scan driver integrated by IZO TFTs including a clock-controlled inverter. J. Disp. Technol. **10**(7), 523–525 (2014)
25. Iñiguez, B., Xu, Z., Fjeldly, T.A., Shur, M.S.: Unified model for short-channel poly-Si TFTs. Solid-State Electron. **43**(10), 1821–1831 (1999)